Reducing Exposure from ^{57}Co Sources During Breast Lymphoscintigraphy by Optimizing Energy Windows and Other Suggested Enhancements of Acquisition and the Display of Images

Borys R. Krynyckyi, MD; Suzana Sata, CNMT; Ian Zolty, CNMT; Chun K. Kim, MD; and Karin Knešaurek, PhD

Division of Nuclear Medicine, Department of Radiology, The Mount Sinai School of Medicine, New York, New York

We set out to measure the reduction in exposure attained by using a weak ^{57}Co sheet source with optimal energy windows. ***Methods:*** Two groups of 10 lymphoscintigraphy studies were analyzed. Group 1 consisted of 10 studies obtained with a stronger source of ^{57}Co, 59 MBq (1.6 mCi) at the time of data acquisition, with transmission images acquired at 3 energy windows of 115–129, 130–134, and 135–150 keV. Group 2 consisted of 10 studies with a weaker sheet source of ^{57}Co, 11 MBq (0.3 mCi). Transmission images were acquired at 3 energy windows of 112–132, 130–134, and 135–150 keV. Same-sized regions of interest (ROIs) were drawn on the patient's torso (PT) and on the nonattenuated image of the transmission source itself (TS), all 1-min images. The counts in each ROI obtained over 1 min and the ratios between the TS ROI and the PT ROI were calculated for all of the energies. Dosimetry calculations based on measured exposure rates and the activity of the sheet sources were used to calculate the patient equivalent dose at 30 cm. ***Results:*** For the ^{57}Co energy window, group 1 had an average ROI count of 1,955 in the TS region and 135 counts in the PT region. The average ratio of TS/PT was 15.4. Similarly, group 2 had an average ROI count of 646.4 in the TS region and 91.2 counts in the PT region. The average ratio of TS/PT was 8.6. The relative "outlining performance," when comparing the ^{57}Co and ^{99m}Tc windows, showed an average improvement when using the ^{57}Co window of 4.4 and 5.8 times for group 1 and group 2, respectively (TS/PT at ^{57}Co window)/(TS/PT at ^{99m}Tc window). Estimates of the patient equivalent dose per study were 2.30 μSv for the stronger ^{57}Co flood source and 0.46 μSv for the weaker ^{57}Co flood source, a 5-fold reduction in equivalent dose. Technologists received less than half of the above doses. ***Conclusion:*** Use of expanded, separate energy windows optimized for the primary 122-keV photon of ^{57}Co greatly improves transmission scan image quality compared with the standard 140-keV ^{99m}Tc windows used for the delineation of the sentinel node. This markedly reduces exposure for all, by allowing the use of a weaker source, and can save time.

Key Words: breast; lymphoscintigraphy; ^{57}Co; exposure; energy windows; display; shield; arm position

J Nucl Med Technol 2004; 32:198–205

Multiple methods of outlining the patient exist with advantages and corresponding disadvantages for each method (*1–5*). Several new ones based on recently introduced acquisition technology exist, including transmission images acquired with a ^{153}Gd line source (97 and 103 keV with additional lower energy γ-rays) that can be superimposed on emission images (*2,3*) and the scout image from SPECT/CT cameras. The scout image would generate less exposure to the patient than a full CT scan and take significantly less time to perform. Conversely, SPECT/CT can provide excellent sentinel node delineation but with added exposure and time. The most popular method continues to be using a ^{57}Co sheet source to generate a transmission scan (*6,7*). However, issues of exposure to both the patient and the technologist as well as time issues have been raised concerning the technique (*2,3*). The suggestion of using alternate energy windows centered at the 122-keV photon for acquisition of ^{57}Co transmission sources and other enhancements has been previously described (*6,7*). We set out to formally quantify the reduction in exposure that optimized energy windows would provide when using ^{57}Co sources of various strengths, whereas maintaining useful transmission images and optimal emission images of the sentinel nodes.

We also describe additional suggested methods of opti-

For correspondence or reprints contact: Borys R. Krynyckyi, MD, Division of Nuclear Medicine, Department of Radiology, Box 1141, The Mount Sinai Medical Center, One Gustave L. Levy Pl., New York, NY, 10029-6574.

E-mail: syrob@msn.com

mizing the acquisition of the images through various maneuvers described at the end of this article.

MATERIALS AND METHODS

The 20 studies (10 in group 1 and 10 in group 2) were performed using our standard injection protocol, which consists of a combination of perilesional and intradermal injections of filtered (Acrodisc syringe filter, 0.2 μm; Pall Corp.) ^{99m}Tc-sulfur colloid as previously described (*1,5,8*). Perilesional injections of 15–30 MBq (400–800 μCi) ^{99m}Tc-sulfur colloid in a volume of 3 mL were administered at ≥2 sites around the lesion at a constantly varying depth. These were followed sequentially by an additional injection of 5.6–15 MBq (150–400 μCi) ^{99m}Tc-sulfur colloid in a volume of 0.6–1.0 mL administered at the areolar cutaneous junction over 1–2 min (*1,5,8*). With the patient supine, the transmission images were obtained as separate 1-min frames in a dynamic sequence after sufficient 1-min-per-frame emission images were acquired for sentinel node delineation, without patient or camera movement.

The cameras used were single-head SPECT Summit Vision 1024RZs (RZ SMV; General Electric Medical Systems) with low-energy, high-resolution, parallel-hole collimators. The intrinsic energy resolution is 9.8% and the crystal thickness is 9.525 mm (0.375 in). The half-life of ^{57}Co is 270.9 d (*9*), and all of the 20 studies were completed within 4 wk of each other, which obviated the need for decay correction.

Three different simultaneous energy windows were acquired (Fig. 1). Group 1 consisted of 10 studies obtained with the stronger source of ^{57}Co, 59 MBq (1.6 mCi), at the time of data acquisition (calibrated at 555 MBq [15 mCi] on April 1, 2001) (Isotope Product Laboratories) with images acquired simultaneously at 3 energy windows of 115–129, 130–134, and 135–150 keV, which represented our old protocol. Emission-only images of the injection site and sentinel nodes were also obtained at these 3 energy windows. Group 2 consisted of 10 studies with a weaker sheet source of ^{57}Co, 11 MBq (0.3 mCi) (calibrated at 370 MBq [10 mCi] on January 25, 2000) (North American Scientific). Transmission images were acquired simultaneously at 3 energy windows of 112–132, 130–134, and 135–150 keV, as were the emission images, in our newer, energy-optimized protocol. The ^{57}Co window was made wider for group 2: from 13% to 16% in our attempt to partly compensate for the lower activity of the weaker ^{57}Co sheet source. The camera systems were automatically peaked with both ^{57}Co (sheet source) and ^{99m}Tc (the injection syringe) simultaneously, in air. The ^{57}Co sheet sources were placed on the floor for anterior views and propped up on a chair at 90° for lateral or oblique views. The patients' bodies were marked on the skin surface with an indelible marker corresponding to the triangulated projection of the sentinel node based on anterior and lateral or oblique camera views to assist the surgeon in further morbidity reduction as previously described (*1,5,10*). Additional standing or sitting emission-only views in the anterior and lateral projections with the arms up over the head and, alternately, out 90° from the long axis of the body in the surgical position were obtained in almost all patients. During the acquisition of the emission images, shields were temporarily placed over the injection sites or sentinel nodes themselves, in some studies, to try to accentuate the sentinel nodes close to the injection site or bring out additional details in nodes closely clustered together. To lessen the negative effects of scatter on sentinel node emission image quality, the upper

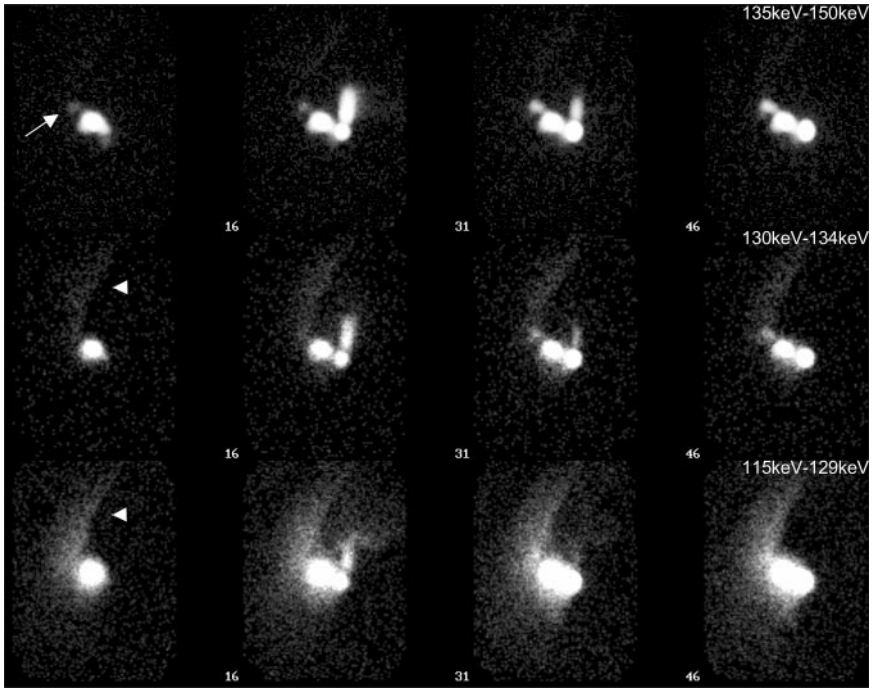

FIGURE 1. Sequence of 10-s frames compressed into 150-s frames at 3 different energy windows acquired simultaneously. Energy window in top row: 135–150 keV. Perilesional injection site and resultant faint sentinel node (arrow). Second through fourth frames (frames 16, 31, and 46) show activity in syringe being injected at areolar cutaneous junction and resultant enhancement of activity in sentinel node "LymphoBoost" (*8*); used for printing of images for the surgeon. Energy window in middle row: 130–134 keV. Scatter from arm (arrowhead) and nonvisualization of sentinel node before and even on or just after second injection. This energy range can contain little useful information and often has excessive scatter so an option exists not to use data in printing images for the surgeon. Energy window in bottom row: 115–129 keV. Nonvisualization of sentinel node on any frame. This energy range can be used for transmission scan with ^{57}Co 122-keV sheet source or for internal body scatter outline (*1,2,5*). It can be printed separately or combined with first row but only if images in top row are also printed as separate images without transmission scan.

energy window (135–150 keV) was used when displaying and printing the emission studies by themselves for the surgeons (*1,5,10*). The transmission images were printed individually from the data collected in the lower ^{57}Co window and also combined with the optimized emission data and also presented to the surgeons. Display settings were adjusted as to the upper and the lower threshold. In addition, adjustment of settings termed "gamma" were done, which represent user-adjustable nonlinear response curves applied to the display, to maximize the delineation of the sentinel node and lymphatic tracts. Additional prescale processing of the data was performed using a built-in function in the workstation, termed "contrast," before applying the color scale map to the data matrix (Vision PowerStation/SMV/GE work station; General Electric Medical Systems) (Fig. 2).

The 2 groups of 10 studies each were analyzed with respect to ^{57}Co transmission source strength, energy windows, transmission image contrast ratios, and both patient and technologist exposure. Same-sized regions of interest (ROIs), 15 × 40 pixels in size, were drawn on the patient torso (PT), avoiding injection sites, lymphatic channels, lymph nodes, and on the nonattenuated image of the transmission source itself (TS) for all 1-min transmission images. The counts were noted in each ROI and the transmission image contrast ratios between the TS ROI and the PT ROI were calculated for all of the energy windows.

Equivalent dose (μSv) to the patients at 30 cm was estimated from the measurements of the exposure rate (mR/h) obtained for both flood sources (Surveyor 2000; Bicron). It was assumed that the f factor (rad/R), as well as the Q factor for γ-rays, were equal to 1.0 (*9*). We also assumed that the patients were not exposed >5 min per study at an average distance of 30 cm.

RESULTS

The results of the individual studies are presented in Table 1. For the ^{57}Co energy window, group 1 had an average ROI count of 1,955 in the TS region and 135 counts in the PT region. The average ratio of TS/PT was 15.4 for group 1. For the ^{57}Co energy window, group 2 had an average ROI count of 646.4 in the TS region and 91.2 counts in the PT region. The average ratio of TS/PT was 8.6 for group 2. The relative "outlining performance," a rough estimate of the improvement in outlining that occurred when using the ^{57}Co energy window as opposed to the standard ^{99m}Tc energy window was defined as (TS/PT at ^{57}Co energy window)/(TS/PT at ^{99m}Tc energy window). This outlining performance was calculated individually for each study and showed an average improvement when using the ^{57}Co energy window of 4.4 and 5.8 times for groups 1 and 2, respectively. For the sheet sources, the relative sensitivity of the cameras at the ^{57}Co energy window compared with the ^{99m}Tc energy window was on average 11.5 times higher. Even when comparing the ratio of TS/PT for the weaker source using the ^{57}Co energy window in group 2 with the ratio of TS/PT for the stronger source using the ^{99m}Tc energy window in group 1 ([TS/PT group 2 using weak ^{57}Co at ^{57}Co energy window]/[TS/PT group 1 using strong ^{57}Co at ^{99m}Tc energy window]), an advantage for the ^{57}Co energy window of >2 times (8.6 vs. 4.2) was present (Table 1).

On the basis of the assumption that the patients were not

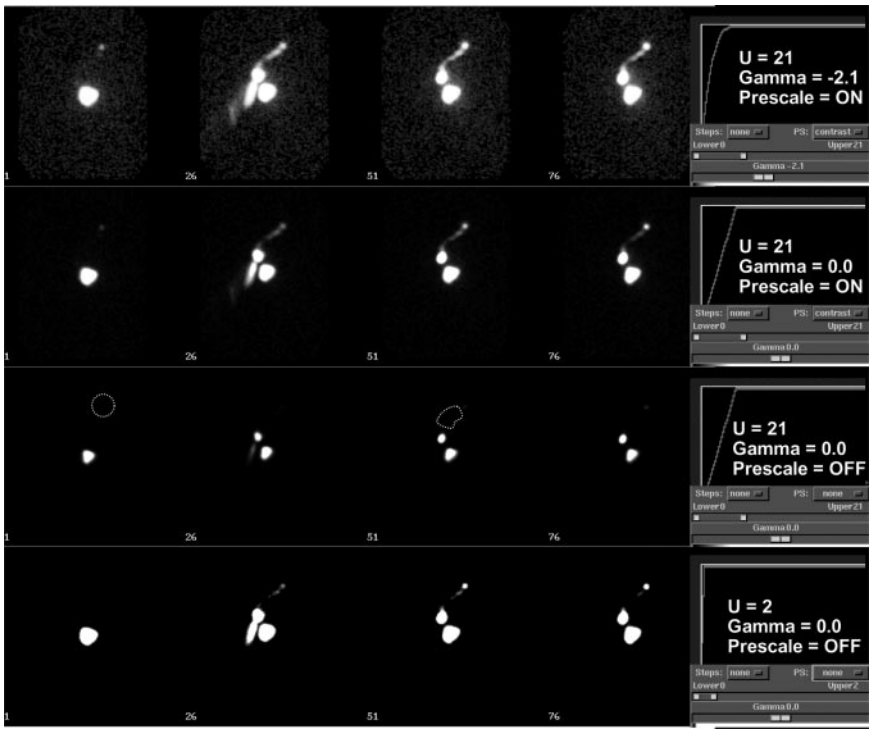

FIGURE 2. Each row of images is of same sequence of 10-s frames compressed into 250-s frames but with different display settings. (Top row) Perilesional injection site and resultant faint sentinel node (frame 1). Second through fourth frames (frames 26, 51, and 76) show activity in syringe being injected at areolar cutaneous junction and resultant lymphatic tract and sentinel node enhancement (*1,5,8*). Optimal settings of prescale data processing enabled a nonlinear γ-curve applied (plot), and upper threshold adjustment allows faint node to be easily seen in frame 1. "Trail" of syringe as it was brought over into field of view (subsequent frame) and lymphatic channel are noted. Second row shows nearly complete loss of the initially faint node and trail as prescaling is turned off. Third row shows switch from γ-response curve to linear response curve (plot), with complete loss of sentinel nodes and lymphatic tracts (dashed ROIs). Bottom row shows attempt to enhance image by adjusting upper threshold to 2, steps away from complete "white out," suboptimal compared with top row.

TABLE 1
ROI Counts Over ^{57}Co Source in Air and Over PT at 3 Energy Windows

Study no.	TS windows			PT windows			TS/PT ratio outlining performance		
	Lower	Middle	Upper	Lower	Middle	Upper	Lower	Middle	Upper
				Group 1					
1	1,776	226	168	131	27	47	13.6	8.4	3.6
2	2,068	157	186	169	12	32	12.2	13.1	5.8
3	2,192	126	208	179	15	57	12.3	8.4	3.7
4	1,643	178	142	136	21	48	12.1	8.5	3.0
5	1,615	115	180	137	9	37	11.8	12.8	4.9
6	2,107	75	157	113	13	37	18.7	5.8	4.2
7	1,945	104	170	133	29	87	14.6	3.6	2.0
8	1,911	170	143	70	7	18	27.3	24.3	8.0
9	2,470	280	221	181	50	155	13.7	5.6	1.4
10	1,818	84	167	101	4	30	18	21	5.6
Average	1,955	151.5	174.2	135	18.7	54.8	15.4	11.1	4.2
± SD	263.1	64.8	25.7	35.1	13.7	38.9	4.8	6.8	1.9
				Group 2					
1	652	25	53	130	17	104	5.0	1.5	0.5
2	650	37	59	67	7	16	9.7	5.3	3.7
3	696	26	52	108	12	56	6.4	2.2	0.9
4	674	46	56	92	16	47	7.3	2.9	1.2
5	612	69	70	53	10	22	11.6	6.9	3.2
6	589	25	58	55	7	22	10.7	3.6	2.6
7	636	46	52	69	7	23	9.2	6.6	2.3
8	693	29	54	167	24	50	4.2	1.2	1.1
9	661	57	51	136	38	102	4.9	1.5	0.5
10	601	31	55	35	6	22	17.7	5.2	2.5
Average	646.4	39.1	56	91.2	14.4	46.4	8.6	3.7	1.8
± SD	37.0	15.1	5.6	42.9	10.1	33.0	4.0	2.2	1.1

Counts are for same-sized ROI (15 × 40 pixels) over patient (PT) and over nonattenuated area of transmission source (TS) for individual group 1 and group 2 studies (n = 10 each). Counts in lower, middle, and upper energy windows in ROI over patient and transmission source are listed for energy windows described in text (group 1: 115–129, 130–134, and 135–150 keV; group 2: 112–132, 130–134, and 135–150 keV). Outlining performance, defined as ratio of counts in ROI over transmission source relative to ROI over patient (TS/PT) for a particular energy window are noted. The higher the ratio the bigger the difference between patient and outlining source and the better the "contrast." Average values of all patients for these indices in each group are presented.

exposed >5 min per procedure (1 min anterior and 1 min oblique or lateral views) and at an average distance of 30 cm, a very conservatively calculated estimate of the patient equivalent dose was 2.30 μSv per study for the stronger ^{57}Co flood source and 0.46 μSv per study for the weaker ^{57}Co flood source. For the stronger flood source, the exposure rate at 30 cm was 2.76 mR/h, which corresponds to an absorbed dose of 0.23 mrad (or 2.3 μGy) for a typical 5-min exposure at 30 cm. The absorbed dose of 2.3 μGy corresponds to an equivalent dose of 2.3 μSv. For the weaker flood source, the exposure rate at 30 cm was 0.55 mR/h and, accordingly, the equivalent dose to the patient for a 5-min exposure at 30 cm was estimated to be 0.46 μSv. Technologists were only exposed during the positioning of the transmission source, approximately 2 min maximum. Therefore, they received much less than half of the patient's equivalent dose.

The transmission images were naturally better, for the stronger ^{57}Co source. However, even with the weak source (with an estimated patient equivalent dose of 0.46 μSv), the images were judged presentable. For the weak source, counts in the TS regions at the ^{57}Co windows were 3.7 times higher compared with the counts for the strong source in the higher optimized ^{99m}Tc energy windows used for sentinel node viewing.

DISCUSSION

The goal of the nuclear medicine imaging specialist in lymphoscintigraphy is to optimally present and accurately delineate the sentinel node(s) to the surgeons using images and triangulated body marking without delaying the surgical schedule. Attention to technique and detail, and the analysis of images in real time to keep track of what is happening, are maneuvers that can be taken to delineate the important nodes in the most accurate and presentable fashion.

Most ^{99m}Tc-based nuclear medicine studies are acquired on a camera with a 20% acceptance window centered around the 140-keV peak γ-energy—that is, 126–154 keV. One disadvantage of this window is the accumulation of

Compton scatter, which adds noise to the images and could hide sentinel nodes. This is especially problematic with the doses of radiotracer used in lymphoscintigraphy studies (essentially a spot infiltration of the entire dose) and the small size and low uptake of the target tissues—that is, the sentinel nodes. By using higher offset energy windows to exclude scatter, the obliterative effects of scatter are reduced (Figs. 1–3). However, disadvantages exist when imaging ^{57}Co sheet sources with upwardly offset energy windows to outline the patient, as the primary photon of ^{57}Co is 122 keV (85.6% abundance) (*9*). Instead of simply using a sheet source with more activity in it, and the resultant increase in exposure, separate optimal energy windows for ^{57}Co are suggested. An additional photon energy of 136.5 keV exists for ^{57}Co, but only with a 10.6% abundance (*9*). The absolute counts in this study were 11.5 times higher for the optimal ^{57}Co windows compared with the optimal windows used to image sentinel nodes, and the "contrast ratios" (TS/PT) were also more favorable (Table 1; Fig. 3). In addition, the ^{57}Co optimized windows allowed the use of a weaker ^{57}Co sheet source and, therefore, reduced exposure, while retaining an acceptable transmission image in most instances. We noted one scenario in which the weaker source would produce suboptimal images, mainly in those patients whose body habitus produced extensive internal scatter from the injection sites. In these patients, the internal body scatter would "fill in" what would normally be the low-count areas of the body on the transmission scan, blurring the outlines. In these instances, printing the transmission images by themselves, not summed or added to any emission-only images, is helpful. Two- to 3-min acquisitions could also be used, when the transmission source is very weak. Alternately, as a last resort, the lower energy scatter images themselves could be used as a rough reference (*4,10*) (Figs. 4 and 5).

The TS/PT ratios were different for the 2 groups: 15.4 and 8.6 for the strong and weak sheet source groups, respectively, at the ^{57}Co window. Several factors could account for this. First, background activity decreases the "ratio" when using the weaker source—that is, background activity has a "relatively" greater contribution to counts in both the PT and TS ROIs when using a weaker source, though this is probably a minor factor. Second, sources of counts in the PT ROI include inherent scatter of activity in the body from the ^{99m}Tc-sulfur colloid injection site, lymphatic tracks, sentinel node, and activity from the ^{57}Co sheet

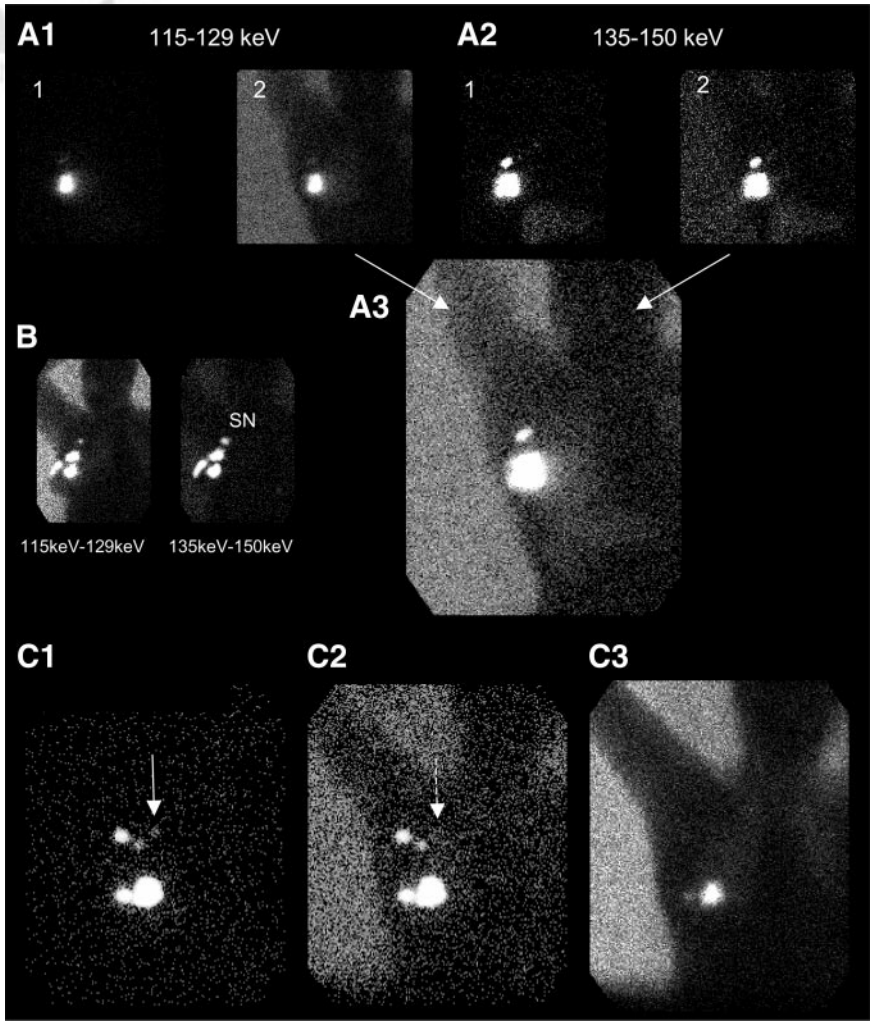

FIGURE 3. (A1) Pair of emission (frame 1) and transmission (frame 2) images at ^{57}Co window. (A2) Pair of emission (frame 1) and transmission (frame 2) images at ^{99m}Tc upwardly offset window for sentinel node delineation. (A3) Combination image created by summing multiple-energy window transmission images from A1 and A2 to produce composite transmission−emission image. (B) Anterior chest at 115- to 129-keV and 135- to 150-keV windows. Counts are higher in ^{57}Co window than in upwardly offset ^{99m}Tc window for optimal sentinel node delineation. (C1 and C2) Sequential emission and transmission images obtained at same ^{99m}Tc upwardly offset window for sentinel node delineation. (C3) Transmission image acquired simultaneously with C2 at ^{57}Co window. Faint node (solid arrow in C1) is "lost" in transmission image (dashed arrow in C2), even at same optimized energy window for sentinel nodes, and illustrates importance of presenting emission-only images. Complete loss of all nodes in ^{57}Co optimized transmission window is evident in C3.

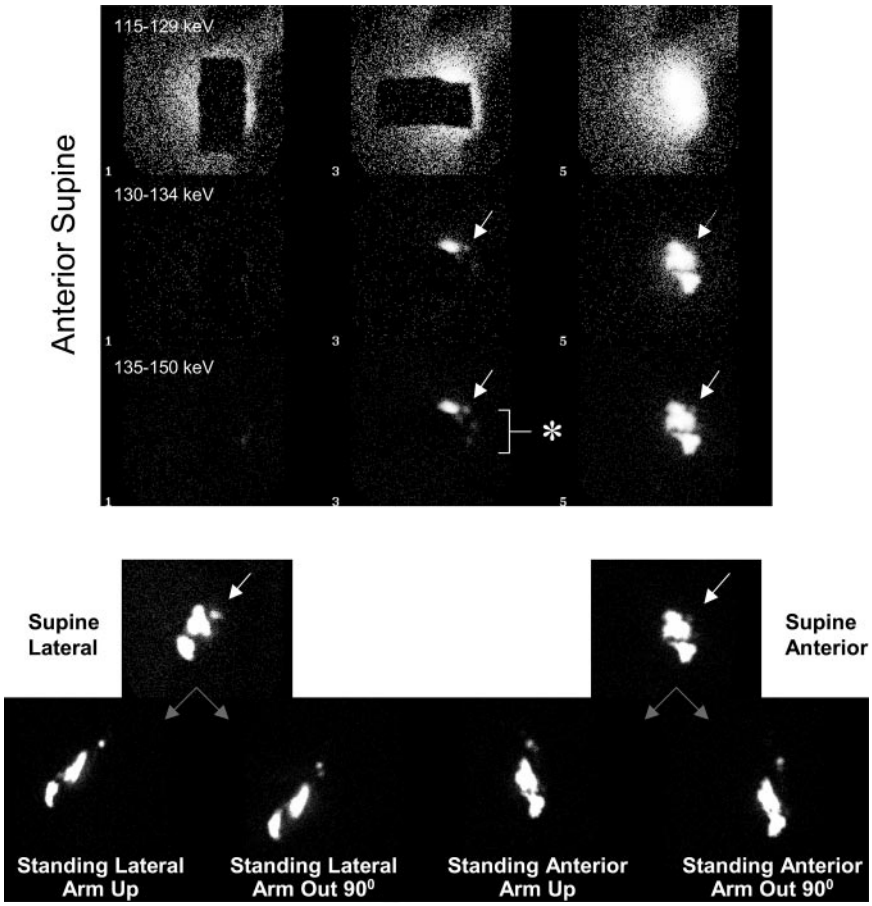

FIGURE 4. Top 3 rows: Sequential anterior images of left chest at 3 energy settings acquired simultaneously. Shielding at 2 different orientations is shown in first 2 columns. (First column) Shielding covers true sentinel node secondary to too much overlap. (Second column) Shielding creates stray foci (bracket and asterisk) that can easily be mistaken to represent true sentinel nodes (arrows). Shielding mainly affects flux with little, if any, effect on scatter reduction. Beneficial effects of scatter reduction are optimal when appropriate energy settings are used (compare second and third rows, arrows pointing to sentinel nodes). Bottom row: Best delineation of nodes occurs with different angled views and standing positions, which shows 2 very closely approximated nodes depending on view.

source that is not attenuated but passes through the patient. The contribution of counts from these sources would be the same whether using weak or strong ^{57}Co sheet sources, except for the contribution of counts from the nonattenuated activity passing though the patient, which would proportionately depend on the source strength. Therefore, when using a weak ^{57}Co sheet source, the relative scatter counts in the PT ROI from the ^{99m}Tc-sulfur colloid injection, lymphatic tracks, and sentinel node will be a proportionately greater percentage of total ROI counts than when a strong source would be used. Finally, the wider lower window used for the weaker source would include more scatter in both TS and PT ROIs but relatively more in the PT ROI from ^{99m}Tc-sulfur colloid. These factors have the effect of reducing the TS/PT ratios in the weak ^{57}Co sheet source group.

The wider variations in the TS counts in group 1 are due to slightly different sheet source-to-camera head distances as well as slight differences in source versus collimator overlap geometry, which appeared to affect the "relative" system sensitivity. Perceived camera sensitivity minimally decreases with increasing distance between the camera and sheet source, about 5% over 40 cm as measured by us. In addition, 2 different cameras of exactly the same model were used with very slightly different inherent sensitivities. Once this was realized, group 2 studies were subsequently performed at a uniform sheet source-to-camera distance and on the same camera, resulting in a slightly "tighter" dataset.

The results show that a 16%, or even wider, window centered at the appropriate energy peak for ^{57}Co will allow the use of a weaker source for the same amount of time while producing adequate (or even superior) transmission images. Concerns have been raised about effective doses of up to 70–210 μSv when using ^{57}Co sheet sources to obtain transmission images during lymphoscintigraphy (as compared with a ^{153}Gd line source), with relatively poor image results at these stated patient exposures (*2,3*). These were most likely not optimized protocols, as ours were, and were lacking in technique, calculation, or measurement of equivalent dose (no ^{57}Co sheet source activity levels are given and the ^{153}Gd window is erroneously stated as 159 keV) or the enhancements discussed in this article (Figs. 1–3). In contrast, Law et al. (*11*), using a female humanoid phantom and thermoluminescent dose meters, had low values for effective patient dose (2.9 μSv) from a ^{57}Co sheet source containing 77 MBq (2.1 mCi) of activity used to generate transmission images, and Sata et al. (*12*) from our group had similar conclusions. As a side note, the edges of transmission sources are "cold" by design. The sources should only be picked up by these edges to minimize exposure to the hands. In addition, tape strips can be applied and fashioned to serve as handles.

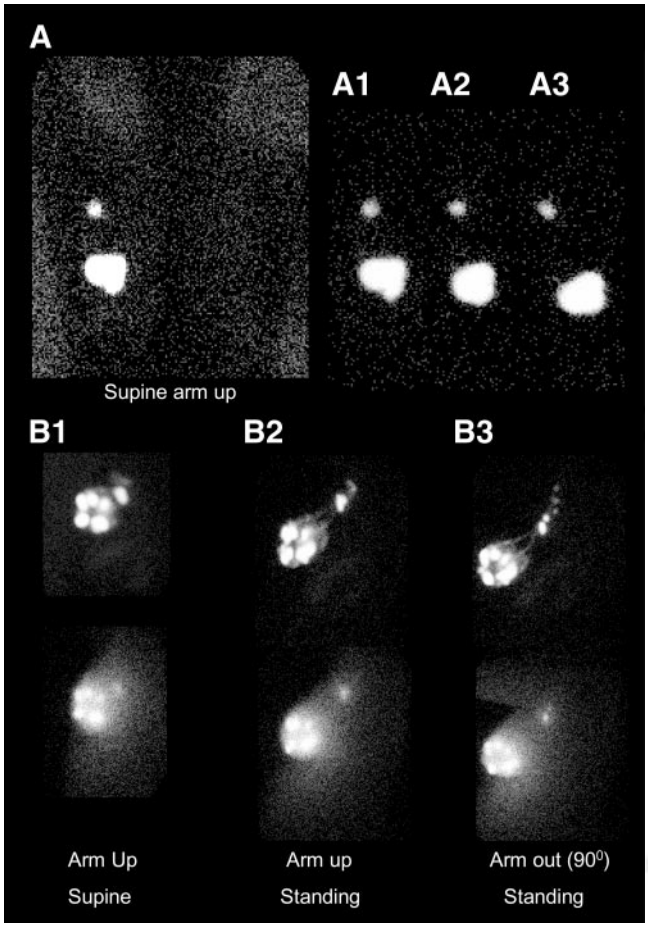

FIGURE 5. Anterior views of patient (A): A1 = Supine, arm up; A2 = Standing, arm up; A3 = Standing, arm out. Distance between injection sites and sentinel node increases and breast tissues shifts inferiorly, anteriorly, and medially as patient's arm is lowered to surgical position and patient assumes standing position. (B1–B3) (Middle row) Lateral views of different patient with 2 lesions in left breast injected at 2 perilesional sites and 2 areolar sites, with activity initially draining through several channels eventually into one. Sentinel nodes and more distant echelon nodes of decreasing intensity are noted. In some supine patients, the raised arm position brings injection sites closer to the axilla and causes nodes to "bunch up," with best separation and delineation often occurring with surgical position (arm 90° out) or with patient standing. (Bottom row) Corresponding body contour scatter images from internal body scatter.

Other Suggestions for Optimal Studies

Display Settings and Presentation of Images. The ability to enhance low-count data for display while suppressing high-count data—that is, avoiding oversaturation of the image from extremely intense injections ("blooming/bleeding") or even nodes—is critical to delineate faint lymphatic channels and faint nodes (Figs. 1–5). In addition to upper and lower threshold settings, adjustment of other display functions is almost always necessary to achieve this—variably referred to as "gamma," "contrast," or "threshold" (Fig. 2). The gamma setting adjustment changes the shape of the gray-scale mapping curve (display vs. matrix data) (Fig. 2). Additional data-processing "prescale" functions (manual or automatic) exist in some cameras. These manipulate the matrix data even before it is mapped to the gray scale, further enhancing the low-count data relative to the high-count data. Digitally masking the injection sites on the postacquisition data is unfortunately necessary on some older systems with limited display control features. Two sets of images are suggested for every view: one with the transmission scan and one without (Fig. 3).

Physical Shielding. Temporarily shielding the injection site or clusters of nodes in the setting of melanoma has been described as increasing the number of detected nodes by a third (*13*). However, our own experience with shielding in breast cancer patients has produced disappointing results (Fig. 4). Shielding the injection site can be very tricky to perform as the positioning is critical; too much overlap by the shield and one can cover the node one is trying to visualize. Too little overlap with the injection site can make interpretation difficult; with activity "peaking" just at or around the lead edges of the shield at multiple points from scatter or the irregular edges of the diffusion or injection field, all of which can appear as "foci" of activity that could be erroneously interpreted as a node(s) (Fig. 4). A partial solution has been suggested in the form of a "graded-shield technique" using a shield composed of 3 concentric layers of increasingly dense leaded plastic (*14,15*). Shielding does not generally reduce scatter from surrounding tissues. Consider the analogy of putting one's hands over the sun; the scatter in the atmosphere from moisture and air molecules that makes the sky bright blue continues to overpower the stars. Shielding does reduce flux from primary and scatter photons from causing collimator-based septal-penetration star artifact, which could "hide" faint adjacent nodes (*16,17*) and can reduce the overload from extreme dynamic range data that can occur with slower camera head electronics or data management systems. The ability to eliminate septal-penetration artifact by using high-quality nonfoil collimators and/or higher offset energy windows, without using lead plates, has also been similarly addressed by others (*6,16,17*).

Patient Arm Position. Arm positioning issues have been addressed in prior articles (*1,5,18–21*), and usually the surgeon and the nuclear medicine physician will have decided on a set of views and arm positions. Sitting or standing views, with the arm out in the 90° surgical position, obtained in the anterior, oblique, or lateral projection, will often displace the injection site further away from the axillary sentinel node and will often further separate the nodes in the axilla into distinct foci (*1,5,18,19*) (Figs. 4 and 5). The raised arm position towards the head above the 90° surgical position can actually decrease the distance between injection site and nodes and cause the nodes to appear to overlap each other. These suggested maneuvers can also reveal nodes close to the injection site that might be obscured by the diffusion zone and can shift "cold" attenuating breast tissues inferiorly to reveal faint echelon nodes, without the need to manually displace the breast or use special wedges for patient positioning (Figs. 4 and 5).

CONCLUSION

Attention to the numerous details of performing lymphoscintigraphy are necessary to obtain the best results. By using the ^{57}Co sheet source for outlining the body contours, reasonable basic anatomic localization is possible. However, without proper window and display settings, the presentation of the images can be suboptimal and, therefore, of limited diagnostic use. The use of additional energy windows for ^{57}Co provides the best possible images, especially important for weak sources of ^{57}Co that minimize exposure to both patient and personnel. We believe that the additional equivalent dose in the general range of <3 μSv (2.30 μSv or 0.46 μSv for the sources in our series at the time of data collection) is certainly reasonable for a ^{57}Co sheet source that can provide excellent images.

REFERENCES

1. Krynyckyi BR, Kim CK, Shafir MK, Mosci K, Machac J. Breast cancer and its management, the utility and technique of lymphoscintigraphy. In: Freeman LM, ed. *Nuclear Medicine Annual.* Philadelphia, PA: Lippincott William & Wilkins; 2003:131–169.
2. Krynyckyi BR, Kim CK, Goyenechea M, Machac J. Methods to outline the patient during lymphoscintigraphy [letter]. *J Nucl Med.* 2003;44:992.
3. Clarke E, Notghi A, Harding K. Improved body-outline imaging technique for localization of sentinel lymph nodes in breast surgery. *J Nucl Med.* 2002;43:1181–1183.
4. Fujii H, Yamashita H, Nakahara T, et al. Outlining the body contours with scattered photons in lymphoscintigraphy for sentinel nodes. *Ann Nucl Med.* 2000;14:401–404.
5. Krynyckyi BR, Kim CK, Goyenechea MR, Chan PT, Zhang ZY, Machac J. Clinical breast lymphoscintigraphy: optimal techniques for performing studies, image atlas, and analysis of images. *Radiographics.* 2004;24:121–145.
6. Keshtgar MRS, Waddington WA, Lakhani SR, Ell PJ. Imaging techniques. In: Keshtgar MRS, Waddington WA, Lakhani SR, et al. *The Sentinel Node in Surgical Oncology.* Berlin, Germany: Springer-Verlag; 1999:66−69, 76.
7. Vallejo Mar M, Gee-Johnson S, Kim EE, Podoloff DA. Whole-body lymphoscintigraphy using transmission scans. *J Nucl Med Technol.* 2002; 30:12–17.
8. Krynyckyi BR, Kim CK, Mosci K, et al. Areolar-cutaneous "junction" injections to augment sentinel node count activity. *Clin Nucl Med.* 2003; 28:97–107.
9. Cherry SR, Sorenson JA, Phelps ME. *Physics in Nuclear Medicine.* 3rd ed. Philadelphia, PA: WB Saunders; 2003:454.
10. Krynyckyi BR, Miner M, Ragonese JM, Firestone M, Kim CK, Machac J. Technical aspects of performing lymphoscintigraphy: optimization of methods used to obtain images. *Clin Nucl Med.* 2000;25:978–985.
11. Law M, Cheng KC, Wu PM, Ho WY, Chow LW. Patient effective dose from sentinel lymph node lymphoscintigraphy in breast cancer: a study using a female humanoid phantom and thermoluminescent dosemeters. *Br J Radiol.* 2003;76:818–823.
12. Sata S, Knesaurek K, Krynyckyi BR. Effective dose in sentinel lymph node imaging [letter]. *Br J Radiol.* 2004;77:709.
13. Maza S, Valencia R, Geworski L, et al. Temporary shielding of hot spots in the drainage areas of cutaneous melanoma improves accuracy of lymphoscintigraphic sentinel lymph node diagnostics. *Eur J Nucl Med Mol Imaging.* 2002;29:1399–1402.
14. Chen YW. Enhanced SLN scintigraphic mapping of breast cancer using graded shields on vertical angle imaging of dual-headed gamma camera. [abstract] *J Nucl Med.* 2002;43(suppl):220P.
15. Chen YW, Lai YC, Hsu CC, Hou MF. Enhanced sentinel lymphoscintigraphic mapping in breast tumor using the graded shield technique. *Kaohsiung J Med Sci.* 2003;19:339–344.
16. Tsushima H, Yamanaga T, Shimonishi Y, Ochi H. Usefulness of imaging method without using lead plate for sentinel lymph node scintigraphy. *Kaku Igaku.* 2002;39:161–169.
17. Uren RF, Howman-Giles R, Thompson JF. Reconfirmation of clinical unpredictability of lymphatic drainage in cutaneous melanoma and new developments in sentinel lymph node diagnostics [reply to letter]. *J Nucl Med.* 2003;44:1871–1872.
18. Uren RF, Howman-Giles R, Renwick SB, Gillett D. Lymphatic mapping of the breast: locating the sentinel lymph nodes. *World J Surg.* 2001;25:789–793.
19. Pierini A, Dworkin HJ. Is the upright position more sensitive than the supine position in breast cancer sentinel node lymphoscintigraphy? *Clin Nucl Med.* 2001;26:823–825.
20. Haigh PI, Hansen NM, Giuliano AE, Edwards GK, Ye W, Glass EC. Factors affecting sentinel node localization during preoperative breast lymphoscintigraphy. *J Nucl Med.* 2000;41:1682–1688.
21. Ichihara H, Kinoshita F, Hiyoshi K, Beppu T, Fujigasaki K. Usefulness of imaging posture using modified oblique view of the axilla (MOVA) for sentinel lymph node scintigraphy in patients with breast cancer. *Nippon Hoshasen Gijutsu Gakkai Zasshi.* 2003;59:765–770.